Applied Physics Letters ARTICLE scitation.org/journal/apl

An electrical thermometry platform for measuring cross-plane thermal conductivity of 2D flakes on substrate

Cite as: Appl. Phys. Lett. **115**, 123102 (2019); doi: 10.1063/1.5118003
Submitted: 2 July 2019 · Accepted: 3 September 2019 ·
Published Online: 17 September 2019

Yu-Chao Hua,[1,a)] Lei Xing,[2,a)] Li-Ying Jiao,[2] and Bing-Yang Cao[1,b)]

AFFILIATIONS

[1]Key Laboratory for Thermal Science and Power Engineering of Ministry of Education, Department of Engineering Mechanics, Tsinghua University, Beijing 100084, People's Republic of China
[2]Key Laboratory of Organic Optoelectronics and Molecular Engineering of the Ministry of Education, Department of Chemistry, Tsinghua University, Beijing 100084, People's Republic of China

[a)]**Contributions:** Y.-C. Hua and L. Xing contributed equally to this work.
[b)]**E-mail:** caoby@tsinghua.edu.cn

ABSTRACT

It is highly desired to efficiently probe the cross-plane thermal conductivities of two-dimensional (2D) flakes with a considerably small temperature increase, avoiding the difficulty of suspending the atomically thin samples. A thermometry platform was proposed for measuring the cross-plane thermal conductivity of irregular dielectric and semiconductor 2D flakes on a substrate. Two metal heaters with identical configurations were fabricated on the same chip, one deposited on the sample and the other was directly on the substrate as a reference. The value of cross-plane thermal conductivity could be derived by fitting the heaters' effective thermal resistances with finite-element-method simulations. The measurement error of the heaters' effective thermal resistances was approximately 1% with the imposed temperature increase of less than 1 K. This platform was used to measure the cross-plane thermal conductivity of WSe_2 2D flakes. The measured values were about eightfold smaller than those of bulk material, which agreed well with the model's predictions.

The study of thermal transport properties of two-dimensional (2D) materials and their stacked structures (e.g., few-layer graphene and transition metal dichalcogenides) has become a research hotspot,[1–10] owing to their great application prospects in electronics, thermoelectrics, and optoelectronics.[11–15] The exfoliation technique has proven to be a powerful technique to produce 2D layered materials.[16,17] However, the exfoliated samples are generally 2D flakes of small area and irregular shape, and it is rather difficult to suspend such atomically thin flakes for the measurement. These issues make the thermal property measurement of 2D layered materials very challenging.

Table I summarizes the relevant measurement techniques. As a noncontact and nondestructive technique, the Raman spectroscopy method has been widely utilized to probe the thermal properties of monolayer and few-layer 2D material flakes.[18–21] The temperature increase within the sample is obtained by detecting the Raman shift, which exhibits a relatively poor accuracy for some materials. Thus, usually a larger temperature increase is required, which could raise concerns about the measurement precision, due to the influence of thermal properties' variation with temperature. Beechem *et al.*[22] discussed this issue in the Raman method in detail. Additionally, the conventional TDTR (time-domain thermoreflectance) technique has been proven to be a powerful tool with which the anisotropic thermal conductivities of bulk and thin-film materials that have a large surface area for depositing the metal transducer are probed.[23–27] In fact, it is not well applicable for monolayer or few-layer 2D material flakes. Regarding this issue, Jang *et al.*[28] demonstrated a modified TDTR method to characterize the anisotropic thermal conductivities of rhenium disulfide flakes with the metal transducers on their top surfaces. Except for the optical methods mentioned above, various electrical methods have been applied to characterize the thermal conductivities of layered materials. Similar to the TDTR method, the conventional 3ω technique is applicable for bulk and thin-film materials rather than 2D flakes of small area and irregular shape.[29–31] The suspended microbridge method exhibits ultrahigh sensitivity and accuracy for in-plane thermal transport,[32] and thus, it can be used to probe the in-plane thermal conductivities of 2D

TABLE I. Relevant measurement techniques and their features.

	Measurement technique	Sensitive properties	Important features
Optical	Raman	In-plane	Applicable for monolayer and ultrathin flakes; relatively poor accuracy for detecting the temperature increase
	TDTR	In/Cr-plane	Applicable for bulk and thin film materials; not well applicable for monolayer or few-layer 2D flakes
Electrical	Suspended microbridge	In-plane	High sensitivity and accuracy; applicable for in-plane thermal transport; complicated fabrication process; fragile platform
	3ω method	In/Cr-plane	Applicable for bulk and thin film materials; not applicable for 2D flakes
	Self-designed heaters	In/Cr-plane	Various designs for measuring thermal properties; usually requiring FEM simulations to extract the target properties

layered materials, such as WSe_2, MoS_2, and $ZrTe_5$.[33–35] However, the complicated fabrication process and the requirement that the sample must be suspended greatly limit the utilization of this method.[36] In addition, some researchers used self-designed supported heaters to measure the thermal properties of 2D materials.[36–38] For example, Bae *et al.*[37] fabricated a thermometry platform to study the size-dependent in-plane thermal conductivity of supported graphene ribbons. Therefore, by properly designing the configurations, the supported heaters can be used to probe the targeted thermal properties with the assistance of finite-element-method (FEM) simulations for running the fitting process, to avoid the difficulty of suspending the atomically thin flakes.

In the present research, we designed and fabricated an electrical thermometry platform to probe the cross-plane thermal conductivity of dielectric and semiconductor 2D flakes on a substrate. Electron-beam lithography was used to define the markers on the growth substrate and then fabricate electrode patterns on selected 2D flakes on the substrate. Here, Cr/Pd (10/100 nm) films were thermally evaporated for contacts. Schematics of the platform are reproduced in Fig. 1(a). Two metal heaters with identical configurations were fabricated on the same chip. One short heater was deposited on the supported 2D flake. It was not necessary to deposit the entire heater on the 2D flake, since the sensitivity analysis demonstrated that a heater with its central part (about half of its full length) on the sample is sensitive enough to characterize the cross-plane thermal conductivity of 2D flakes. Another metal heater of the same configuration was directly fabricated on the substrate as a reference. The four-probe method was employed to measure the electrical resistance of the heaters to derive the average temperature increase. Therefore, four metal pads were necessary as shown in Fig. 1(a), and the additional two metal pads were designed for symmetry and as a double-check. Moreover, Fig. 1(b) illustrates the electrical circuit, which is identical to that in the conventional 3ω method. We used a current source (Keithley 6221 DC and AC source) to provide the driving current of low frequency, and a lock-in amplifier (Model SR830) was used to record the 3ω voltage signals.

The heater's effective thermal resistance was calculated as

$$R_{\mathrm{th}} = \frac{\Delta T_{\mathrm{ave}}}{Q_{\mathrm{heater}}}, \tag{1}$$

where ΔT_{ave} is the average temperature increase in the heater and Q_{heater} the heating power within the heater. We measured the effective thermal resistances of the reference heater and the heater on the sample, and the sample's cross-plane thermal conductivity could be derived by fitting the measured effective thermal resistances with the FEM results. For measuring the effective thermal resistance, the heating power could be easily calculated using the electric resistance and driving current, and thus, the key point accurately characterized the temperature increase. Lu *et al.*[39] demonstrated that the module of temperature oscillation within a conductive suspended wire with oscillating Joule heating becomes nearly the same as the temperature

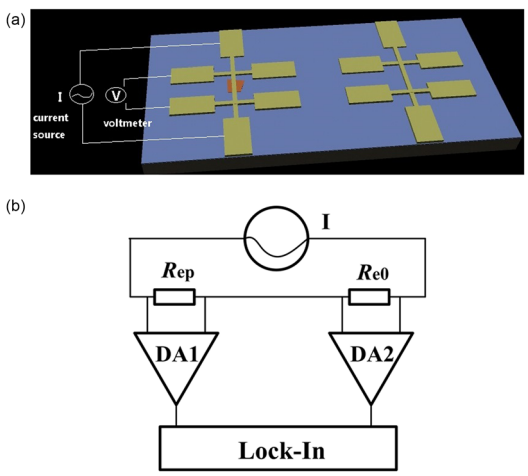

FIG. 1. (a) Schematic of electrical thermometry platform; (b) corresponding electrical circuit diagram, in which R_{e0} is the heater's electric resistance, R_{ep} is the electrical resistance of a paired resistor, and DA denotes the differential amplifier.

increase in the steady-state case when the heating frequency is low enough. Thus, the heater's average temperature increase in the steady state can be derived from the measured the 3ω voltage signals ($V_{3\omega}$) with a low-frequency heating current ($I_{1\omega}$), the frequency of which is equal to 1ω; that is,

$$\Delta T_{\text{ave}} = \frac{2V_{3\omega}}{I_{1\omega}\beta R_{\text{e0}}}, \tag{2}$$

where β is the temperature coefficient of resistance (TCR). Although we used $V_{3\omega}$ to derive the temperature increase, the present platform basically exhibits two differences compared to the conventional 3ω method. First, its heaters' lengths should be comparable to the size of the flakes to guarantee that most of the generated heat can go through the samples, and thus, the heaters were much shorter than in the conventional 3ω method. Second, the conventional 3ω method always records a sequence of 3ω signals varying the frequency, while we merely recorded the 3ω signals at the low frequency to obtain the temperature increase at the steady state.

As a test example, we conducted the FEM simulations to determine whether the method described above was valid for our platform; the substrate was set as a SiO_2 (300 nm)/Si (450 μm) substrate, and the cross-plane and in-plane thermal conductivities of the sample (20 nm thick) were set as 0.1 and 10 W/m K, respectively. As illustrated in Fig. 2(a), the modules of the temperature oscillations were nearly independent of the current frequency (half of the heating frequency) and identical to the steady-state temperature increases when the reciprocal of the current frequency was higher than 0.01 s in the cases of both the reference heater and the heater on the sample.

We then analyzed the sensitivity of the present method. The sensitivity is characterized by the dimensionless sensitivity of the target parameter, and it is given by $s_i = \partial \ln(\kappa_{\text{cr}})/\partial \ln(x_i)$, in which κ_{cr} is the sample's cross-plane thermal conductivity and x_i the measured (or input) parameter. The dimensionless sensitivity was calculated numerically by giving a small perturbation of x_i around its value and rerunning the extraction simulation to derive the variation of cross-plane thermal conductivity. We calculated the dimensionless sensitivity of κ_{cr} with respect to the heater's effective thermal resistance (R_{th}), which is denoted as $|s_{R_{\text{th}}}|$. As shown in Fig. 2(b), the cross-plane thermal conductivity was found to be very sensitive to the heater's effective thermal resistance. Regardless of the value of in-plane thermal conductivity (κ_{in}), the absolute value of the dimensionless sensitivity increased with decreasing cross-plane thermal resistance of unit area, which is given by $r_{\text{cr}} = t_{\text{sam}}/\kappa_{\text{cr}}$, where t_{sam} is the sample's thickness.

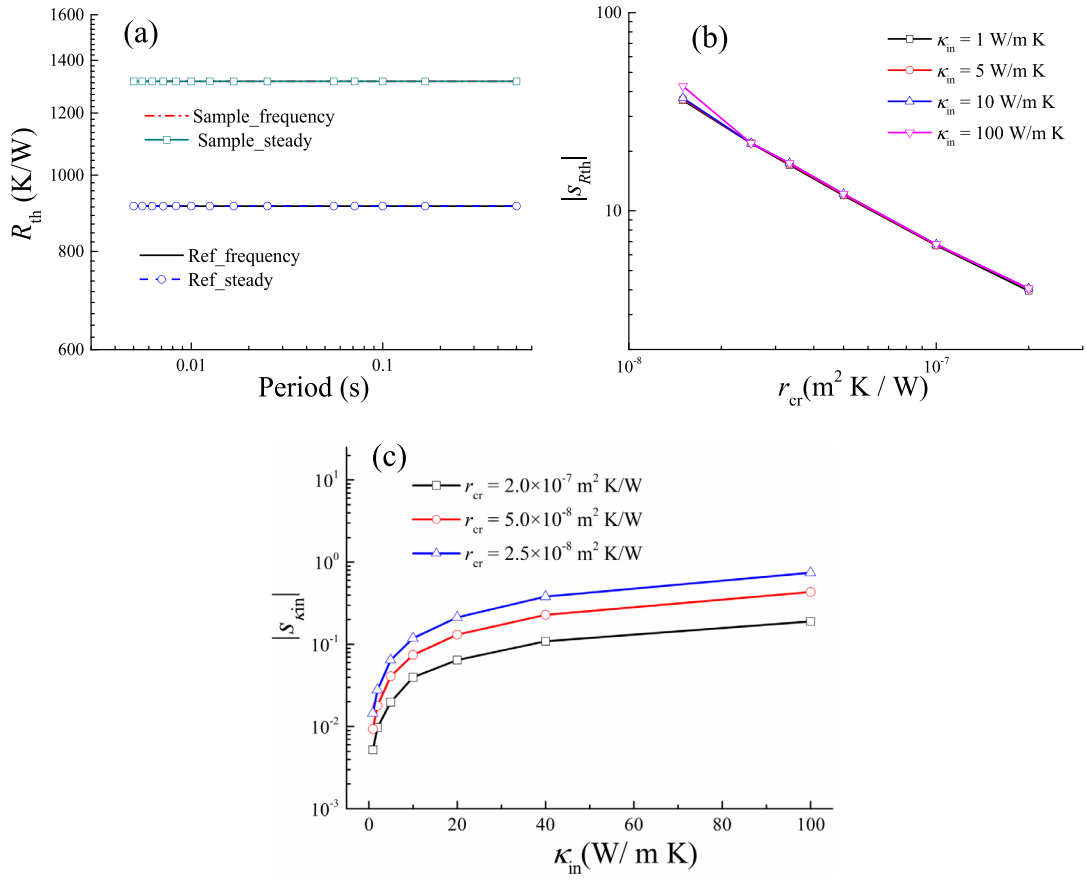

FIG. 2. (a) Effective thermal resistances determined by FEM; absolute values of dimensionless sensitivity of cross-plane thermal conductivity (κ_{cr}) with respect to (b) the heater's effective thermal resistance (R_{th}) and (c) the in-plane thermal conductivity (κ_{in}).

Additionally, in a specific range, the variation of in-plane thermal conductivity had a minor influence on the dimensionless sensitivity with respect to the effective thermal resistance, indicating that the influence of the setting value of in-plane thermal conductivity could be negligible during the fitting process. To further demonstrate this point, we calculated the dimensionless sensitivity of κ_{cr} with respect to κ_{in}, which is denoted as $s_{\kappa_{in}}$. As shown in Fig. 2(c), the absolute value of $s_{\kappa_{in}}$ was considerably small. We could estimate the measurement range via the sensitivity analysis of $s_{R_{th}}$. As $r_{cr} = 2.5 \times 10^{-8}$ m^2 K/W and $\kappa_{in} = 100$ W/m K, $|s_{R_{th}}|$ reached approximately 20. We estimated that the lowest cross-plane thermal resistance of unit area that can be probed with an error of less than 50% is approximately 2.5×10^{-8} m^2 K/W. Nevertheless, according to Refs. 9, 37, and 40, the interfacial thermal resistance of unit area between the 2D material sample and substrate (r_{sam_SiO2}) is on the order of 1.0×10^{-8} m^2 K/W, and thus, r_{sam_SiO2} could be comparable to r_{cr} (the dimensionless sensitivity with respect to r_{sam_SiO2} reached approximately 0.4). In fact, the measured cross-plane thermal conductivity should be an effective value involving the influence of interfacial thermal resistance.

We employed the present method to measure the cross-plane thermal conductivities of WSe_2 2D flakes on the SiO_2/Si substrate. High-quality layered crystals of WSe_2 were mechanically exfoliated from bulk using scotch tape (see supplementary material S.1) and then transferred onto clean silicon substrates covered with 300-nm-thick SiO_2, as shown in Figs. 3(a) and 3(b). The thicknesses of the WSe_2 flakes were 21 nm (sample 1) and 49 nm (sample 2) as measured by atomic-force microscopy (AFM) in contact mode (Fig. S1). A heater was deposited on the 2D flake, and a reference heater was also fabricated on the same substrate, as shown in Figs. 3(c) and 3(d). Electrical contacts were fabricated using electron-beam lithography followed by deposition of 10 nm chromium/100 nm palladium electrodes (see supplementary material S.2).

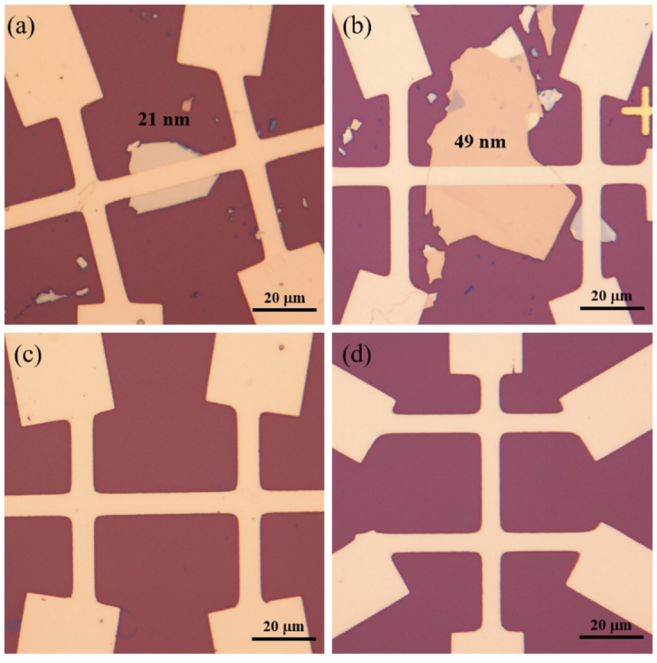

FIG. 3. [(a) and (b)] Optical microscopy image of 21 nm and 49 nm WSe_2 electrical thermometry platforms on the SiO_2/Si substrate, respectively. (c) and (d) Blank electrical thermometry platforms, used as a reference for the measurement of 21 nm and 49 nm WSe_2, respectively.

The cross-plane thermal conductivities of the WSe_2 2D flakes were derived from the measured effective thermal resistances (see supplementary material S.3) by fitting with the FEM simulation results (see supplementary material S.4). As shown in Fig. 4, at 300 K, the cross-plane thermal conductivities of the 21- and 49-nm-thick WSe_2 2D flakes were found to be 0.194 ± 0.026 and 0.227 ± 0.015 W/m K, respectively (see supplementary material S.5 for error analysis), which were significantly smaller than the bulk value (approximately 1.5 W/m K),[23,26,41] which should be attributed to the size confinement in the cross-plane direction.[42–44] The experiments of Muratore *et al.*[41] also demonstrated that the cross-plane thermal conductivity of the WSe_2 nanofilm with a turbostratic structure, the domain size of which was approximately 9 nm, can be reduced to approximately 0.1 W/m K.

A thermal conductivity model was developed in this case, and the $\hat{s}$ directional thermal conductivity is given by

$$\kappa_{\hat{s}} = \int_0^{2\pi} d\varphi \int_{-1}^{1} d\mu \sum_j \int_0^{q_{m,j}} \kappa_{q,j,\hat{s}} q^2 dq, \tag{3}$$

with

$$\kappa_{q,j,\hat{s}} = \left(\hat{s} \cdot \vec{v}_{gj}\right)^2 \tau_{q,j} C_q,$$

where $\vec{v}_{gj}$ is the group velocity, C_q the mode heat capacity, and $\tau_{q,j}$ the relaxation time (see supplementary material S.6). The model predicted cross-plane thermal conductivity values of 0.17 W/m K (21 nm) and 0.2 W/m K (49 nm) for WSe_2 at 300 K, which agreed well with our experimental results. When the scattering length was set to 9 nm, the

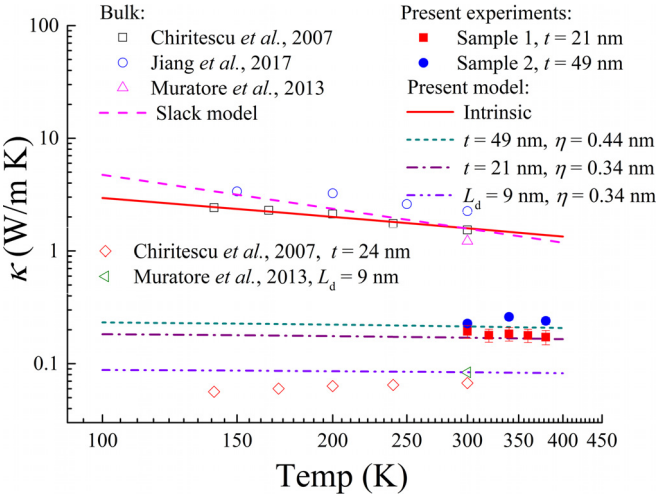

FIG. 4. Cross-plane thermal conductivities of WSe_2 2D flakes vs temperature. The data are: Reproduced with permission from Muratore *et al.*, Appl. Phys. Lett. **102**(8), 081604 (2013). Copyright 2013 AIP Publishing. Reproduced with permission from Chiritescu *et al.*, Science **315**(5810), 351 (2007). Copyright 2007 The American Association for the Advancement of Science. Reproduced with permission from Jiang *et al.*, Adv. Mater. **29**(36), 1701068 (2017). Copyright 2017 John Wiley and Sons.

model could also explain the value reported by Muratore *et al.*[41] Referring to the experimental data and model's predictions, the cross-plane thermal conductivity of 2D WSe_2 flakes could increase with the increasing scattering length. Nevertheless, the measured values for a 24-nm-thick disordered WSe_2 nanofilm by Chiritescu *et al.*[23] were only approximately 0.07 W/m K, which were much lower than our results and model predictions. This was because the disordered structure further reduced the thermal conductivity of the disordered WSe_2 nanofilm. In addition, Fig. 4 shows that our measured thermal conductivities decrease very slightly with increasing temperature. As demonstrated by previous experiments,[26] the Slack model,[41] and our present model, the cross-plane thermal conductivities of bulk WSe_2 also decreased with increasing temperature. The temperature dependence of bulk WSe_2 was reduced compared to the case of 2D flakes, since the phonon-transport process within the 2D flakes should be dominated by boundary scattering.

In summary, an efficient scheme was developed for measuring the cross-plane thermal conductivity of dielectric and semiconductor 2D flakes on a substrate. A supported electrical thermometry platform was designed, and the sample's cross-plane thermal conductivity could be derived from the measured effective thermal resistances of heaters by fitting with the FEM simulation results. This measurement platform is easily fabricated and well applicable for 2D flakes of small area and irregular shape. The measurement error of the heaters' effective thermal resistances was approximately 1% with the imposed temperature increase of less than 1 K, and the lowest cross-plane thermal resistance of unit area that can be probed with a thermal conductivity uncertainty of less than 50% is approximately 2.5×10^{-8} m^2 K/W with an in-plane thermal conductivity of less than 100 W/m K. This method was utilized to measure the cross-plane thermal conductivity of the WSe_2 2D flakes, and a strong boundary-scattering effect was identified. Moreover, those measured values could be well predicted by the thermal conductivity model for the thin layered materials involving the phonon-boundary-scattering effect. The present work can provide an alternative method to efficiently characterize the cross-plane thermal conductivity of dielectric and semiconductor 2D flakes on a substrate.

See the supplementary material for the details of sample preparation, fabrication of the thermometry platform, measurements, simulation of extraction of thermal conductivities, error analysis, and thermal conductivity model of thin layered materials.

This work was financially supported by the National Natural Science Foundation of China (Nos. 51825601, 51676108, 21573125, and 21875127), Initiative Postdocs Supporting Program of China Postdoctoral Science Foundation (No. BX20180155), Project funded by China Postdoctoral Science Foundation (No. 2018M641348), Tsinghua University Initiative Scientific Research Program, and Science Fund for Creative Research Group (No. 51321002).

REFERENCES

[1]D. G. Cahill, P. V. Braun, G. Chen, D. R. Clarke, S. Fan, K. E. Goodson, P. Keblinski, W. P. King, G. D. Mahan, A. Majumdar, H. J. Maris, S. R. Phillpot, E. Pop, and L. Shi, Appl. Phys. Rev. **1**(1), 011305 (2014).
[2]H. Bao, J. Chen, X. Gu, and B.-Y. Cao, ES Energy Environ. **1**, 16 (2018).
[3]M. Ohnishi and J. Shiomi, APL Mater. **7**(1), 013102 (2019).
[4]G. Xie, Z. Ju, K. Zhou, X. Wei, Z. Guo, Y. Cai, and G. Zhang, npj Comput. Mater. **4**(1), 21 (2018).
[5]G. Xie, D. Ding, and G. Zhang, Adv. Phys.: X **3**(1), 1480417 (2018).
[6]Y. Wang, N. Xu, D. Li, and J. Zhu, Adv. Funct. Mater. **27**(19), 1604134 (2017).
[7]L. Qiu, P. Guo, H. Zou, Y. Feng, X. Zhang, S. Pervaiz, and D. Wen, ES Energy Environ. **2**, 66 (2018).
[8]C. Liu, M. Chen, W. Yu, and Y. He, ES Energy Environ. **2**, 31 (2018).
[9]Y. K. Koh, M.-H. Bae, D. G. Cahill, and E. Pop, Nano Lett. **10**(11), 4363 (2010).
[10]Z. Luo, J. Maassen, Y. Deng, Y. Du, R. P. Garrelts, M. S. Lundstrom, P. D. Ye, and X. Xu, Nat. Commun. **6**, 8572 (2015).
[11]M. Osada and T. Sasaki, Adv. Mater. **24**(2), 210 (2012).
[12]K. S. Novoselov, A. Mishchenko, A. Carvalho, and A. H. Castro Neto, Science **353**(6298), aac9439 (2016).
[13]J. Zheng, X. Yan, Z. Lu, H. Qiu, G. Xu, X. Zhou, P. Wang, X. Pan, K. Liu, and L. Jiao, Adv. Mater. **29**(13), 1604540 (2017).
[14]L. Liu, J. Wu, L. Wu, M. Ye, X. Liu, Q. Wang, S. Hou, P. Lu, L. Sun, J. Zheng, L. Xing, L. Gu, X. Jiang, L. Xie, and L. Jiao, Nat. Mater. **17**(12), 1108 (2018).
[15]Q. Zhang, X.-F. Wang, S.-H. Shen, Q. Lu, X. Liu, H. Li, J. Zheng, C.-P. Yu, X. Zhong, L. Gu, T.-L. Ren, and L. Jiao, Nat. Electron. **2**(4), 164 (2019).
[16]L. Ottaviano, S. Palleschi, F. Perrozzi, G. D'Olimpio, F. Priante, M. Donarelli, P. Benassi, M. Nardone, M. Gonchigsuren, M. Gombosuren, A. Lucia, G. Moccia, and O. A. Cacioppo, 2D Mater. **4**(4), 045013 (2017).
[17]N. Wang, Q. Xu, S. Xu, Y. Qi, M. Chen, H. Li, and B. Han, Sci. Rep. **5**, 16764 (2015).
[18]H. Malekpour and A. A. Balandin, J. Raman Spectrosc. **49**(1), 106 (2018).
[19]R. Yan, J. R. Simpson, S. Bertolazzi, J. Brivio, M. Watson, X. Wu, A. Kis, T. Luo, A. R. Hight Walker, and H. G. Xing, ACS Nano **8**(1), 986 (2014).
[20]R. Wang, T. Wang, H. Zobeiri, P. Yuan, C. Deng, Y. Yue, S. Xu, and X. Wang, Nanoscale **10**(48), 23087 (2018).
[21]Q. Cai, D. Scullion, W. Gan, A. Falin, S. Zhang, K. Watanabe, T. Taniguchi, Y. Chen, E. J. G. Santos, and L. H. Li, Sci. Adv. **5**(6), eaav0129 (2019).
[22]T. Beechem, L. Yates, and S. Graham, Rev. Sci. Instrum. **86**(4), 041101 (2015).
[23]C. Chiritescu, D. G. Cahill, N. Nguyen, D. Johnson, A. Bodapati, P. Keblinski, and P. Zschack, Science **315**(5810), 351 (2007).
[24]J. P. Feser, J. Liu, and D. G. Cahill, Rev. Sci. Instrum. **85**(10), 104903 (2014).
[25]W.-P. Hsieh, B. Chen, J. Li, P. Keblinski, and D. G. Cahill, Phys. Rev. B **80**(18), 180302(R) (2009).
[26]P. Jiang, X. Qian, X. Gu, and R. Yang, Adv. Mater. **29**(36), 1701068 (2017).
[27]P. Jiang, X. Qian, and R. Yang, J. Appl. Phys. **124**(16), 161103 (2018).
[28]H. Jang, C. R. Ryder, J. D. Wood, M. C. Hersam, and D. G. Cahill, Adv. Mater. **29**(35), 1700650 (2017).
[29]C. Dames and G. Chen, Rev. Sci. Instrum. **76**(12), 124902 (2005).
[30]D. G. Cahill, Rev. Sci. Instrum. **75**(12), 5119 (2004).
[31]Y. K. Koh, S. L. Singer, W. Kim, J. M. O. Zide, H. Lu, D. G. Cahill, A. Majumdar, and A. C. Gossard, J. Appl. Phys. **105**(5), 054303 (2009).
[32]L. Shi, D. Li, C. Yu, W. Jang, D. Kim, Z. Yao, P. Kim, and A. Majumdar, J. Heat Transfer **125**(5), 881 (2003).
[33]A. Mavrokefalos, N. T. Nguyen, M. T. Pettes, D. C. Johnson, and L. Shi, Appl. Phys. Lett. **91**(17), 171912 (2007).
[34]A. Aiyiti, X. Bai, J. Wu, X. Xu, and B. Li, Sci. Bull. **63**(7), 452 (2018).
[35]J. Guo, Y. Huang, X. Wu, Q. Wang, X. Zhou, X. Xu, and B. Li, Phys. Status Solid RRL **13**(3), 1800529 (2019).
[36]Z. Li, M.-H. Bae, and E. Pop, Appl. Phys. Lett. **105**(2), 023107 (2014).
[37]M. H. Bae, Z. Li, Z. Aksamija, P. N. Martin, F. Xiong, Z. Y. Ong, I. Knezevic, and E. Pop, Nat. Commun. **4**, 1734 (2013).
[38]P. Yasaei, C. J. Foss, K. Karis, A. Behranginia, A. I. El-Ghandour, A. Fathizadeh, J. Olivares, A. K. Majee, C. D. Foster, F. Khalili-Araghi, Z. Aksamija, and A. Salehi-Khojin, Adv. Mater. Interfaces **4**(17), 1700334 (2017).
[39]L. Lu, W. Yi, and D. L. Zhang, Rev. Sci. Instrum. **72**(7), 2996 (2001).
[40]H. Zhou and G. Zhang, Chin. Phys. B **27**(3), 034401 (2018).
[41]C. Muratore, V. Varshney, J. J. Gengler, J. J. Hu, J. E. Bultman, T. M. Smith, P. J. Shamberger, B. Qiu, X. Ruan, A. K. Roy, and A. A. Voevodin, Appl. Phys. Lett. **102**(8), 081604 (2013).
[42]Y.-C. Hua and B.-Y. Cao, Int. J. Therm. Sci. **101**, 126 (2016).
[43]Y.-C. Hua and B.-Y. Cao, Nanoscale Microscale Thermophys. Eng. **21**(3), 159 (2017).
[44]Y.-C. Hua, H.-L. Li, and B.-Y. Cao, IEEE Trans. Electron Devices **66**(8), 3296–3301 (2019).